Flexibility of a biotinylated ligand in artificial metalloenzymes based on streptavidin – an insight from Molecular Dynamics simulations with classical and *ab initio* force fields

Jarosław J. Panek[1*], Thomas R. Ward[2], Aneta Jezierska-Mazzarello[1,3], Marjana Novič[3]

[1]University of Wrocław, Faculty of Chemistry, ul. F. Joliot-Curie 14, 50-383 Wrocław, Poland
[2] University of Basel, Department of Chemistry, Spitalstrasse 51, CH-4056 Basel, Switzerland
[3] National Institute of Chemistry, Hajdrihova 19, SI-1001 Ljubljana, Slovenia

***Corresponding author:** Jarosław J. Panek, e-mail: jarek@elrond.chem.uni.wroc.pl, phone: +48 71 3757 246, Fax: +48 71 3282348

ONLINE RESOURCE 2

Table of contents:

SAV and its mutants.

14. Solvent accessible surface area (SASA) calculated as a function of simulation time for WT SAV and WT SAV-biotin and its mutants with biotin.
15. Solvent-accessible surface area (SASA) calculated as a function of simulation time for WT SAV, WT SAV-[η^6-(*p*-cymene)Ru(Biot-*p*-L)Cl] and its mutants with [η^6-(*p*-cymene)Ru(Biot-*p*-L)Cl].
16. Time evolution of the Ru-Ru distances for metals in neighboring η^6-(p-cymene)Ru(Biot-*p*-L)Cl ligands anchored in WT SAV. Results of classical MD.
17. Time evolution of the Ru-Ru distances for metals in neighboring η^6-(p-cymene)Ru(Biot-*p*-L)Cl ligands anchored in S112A-SAV. Results of classical MD.
18. Time evolution of the Ru-Ru distances for metals in neighboring η^6-(p-cymene)Ru(Biot-*p*-L)Cl ligands anchored in S112K-SAV. Results of classical MD.
19. Time evolution of the Ru-Ru distances for metals in neighboring η^6-(p-cymene)Ru(Biot-*p*-L)Cl ligands anchored in P64G-SAV. Results of classical MD.
20. Additional view of the biotin surrounded by selected residues forming hydrogen bonding network – a model for *ab initio* Born-Oppenheimer Molecular Dynamics.
21. Additional view of the biotin surrounded by selected residues forming hydrogen bonding network – a model for *ab initio* Born-Oppenheimer Molecular Dynamics. Fixed atoms are indicated.
22. Time evolution of the hydrogen bonds with carbonyl oxygen atom of biotin acting as an acceptor. Results of classical force field molecular dynamics for the P64G SAV mutant loaded with the metal-bearing cofactor
23. Time evolution of the hydrogen bonds with the N2 ureido nitrogen atom of biotin acting as a donor. The acceptor atoms are two carboxyl oxygens of Asp128. Results of classical force field molecular dynamics for the S112K SAV mutant loaded with the metal-bearing cofactor.
24. Time evolution of the two hydrogen bonds: with the N1 ureido nitrogen atom of biotin acting as a donor (N1-H…O-Ser45) and the sulfur atom of the biotin acting as an acceptor (Ser90-O-H…S). Results of classical force field molecular dynamics for the S112K SAV mutant loaded with the metal-bearing cofactor.

Discussion of RMSF and SASA parameters for the studied structures.

The stability of the SAV scaffold on the local scale is visible in the graphs representing the Root Mean Square Fluctuation (RMSF) of the backbone carbon atoms (Figures SI10 – SI12 of this Online Resource 2). Data for full tetramer are shown. No significant difference in the RMSF is observed between the four apo structures. This underlines the most important point of the classical dynamics part of this study: point mutations did not affect significantly the overall dynamics of the protein backbone. This is true on the global as well as local scale. A similar behavior is recorded also for the biotin- or cofactor-loaded SAV variants. This suggests that the modifications leading to the changes of the catalytic activity must be connected with the local environment of the metal, and not with backbone dynamics.

Solvent-Accessible Surface Area (SASA) is a parameter facilitating analysis of the interaction between studied cofactor-protein complexes and water. This parameter helps to detect unusual events e.g.: closing or opening of the pockets in the studied protein. Its time dependence during classical MD runs for the considered structures is presented in Figures SI13, SI14 and SI15. In the case of apo structures (Figure SI13), the graphs are similar, but the S112K SAV has significantly larger solvent-accessible surface areas. This is consistently observed also for the cofactor-loaded protein structures (Fig. SI14, SI15). Summarizing, variations of the SASA during the simulation do not mark any of the protein variants as having significantly disturbed solvation structure.

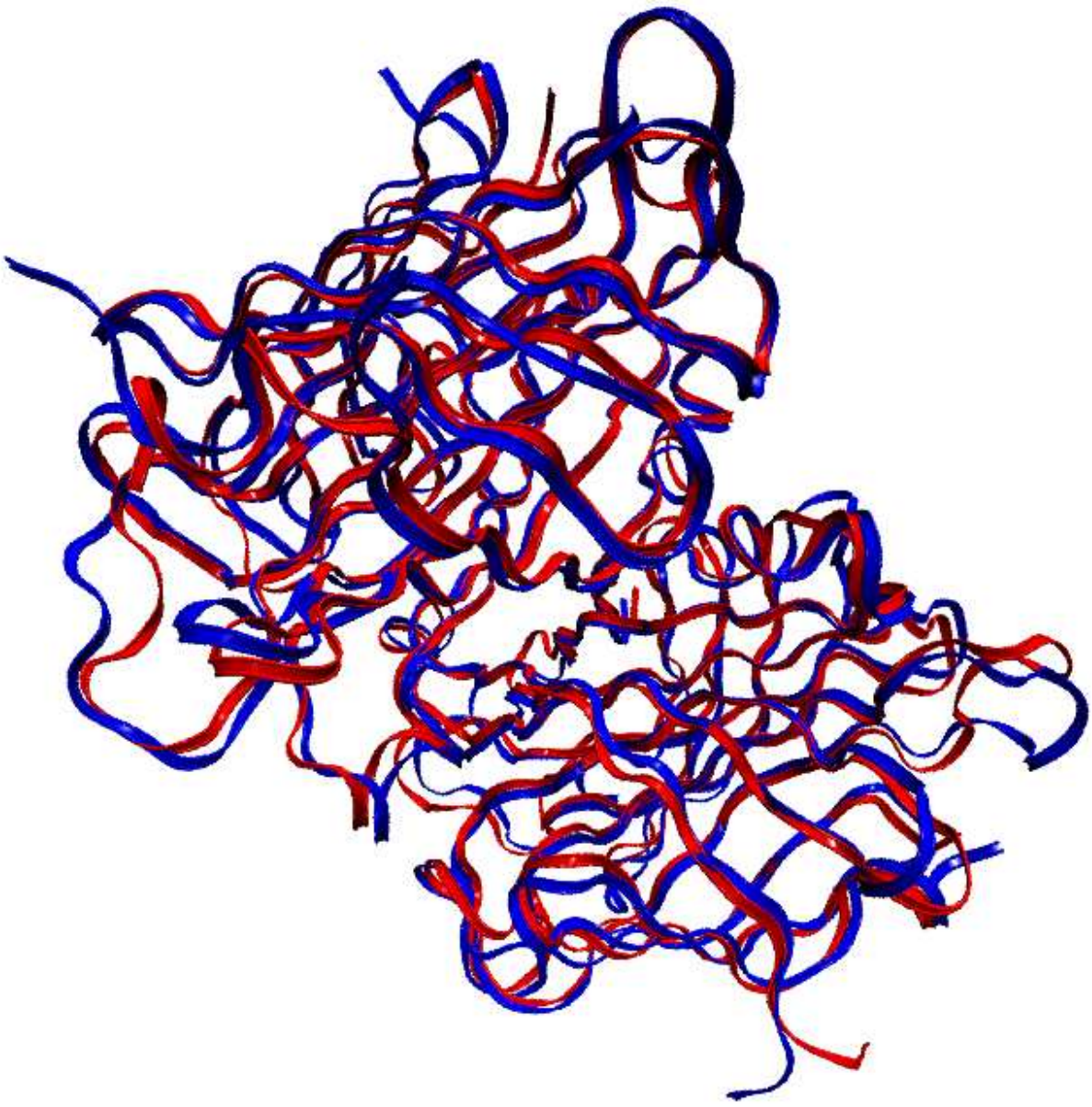

Fig. SI1 Superimposition of the WT SAV before (red color) and after 56 ns of the MD run (blue color)

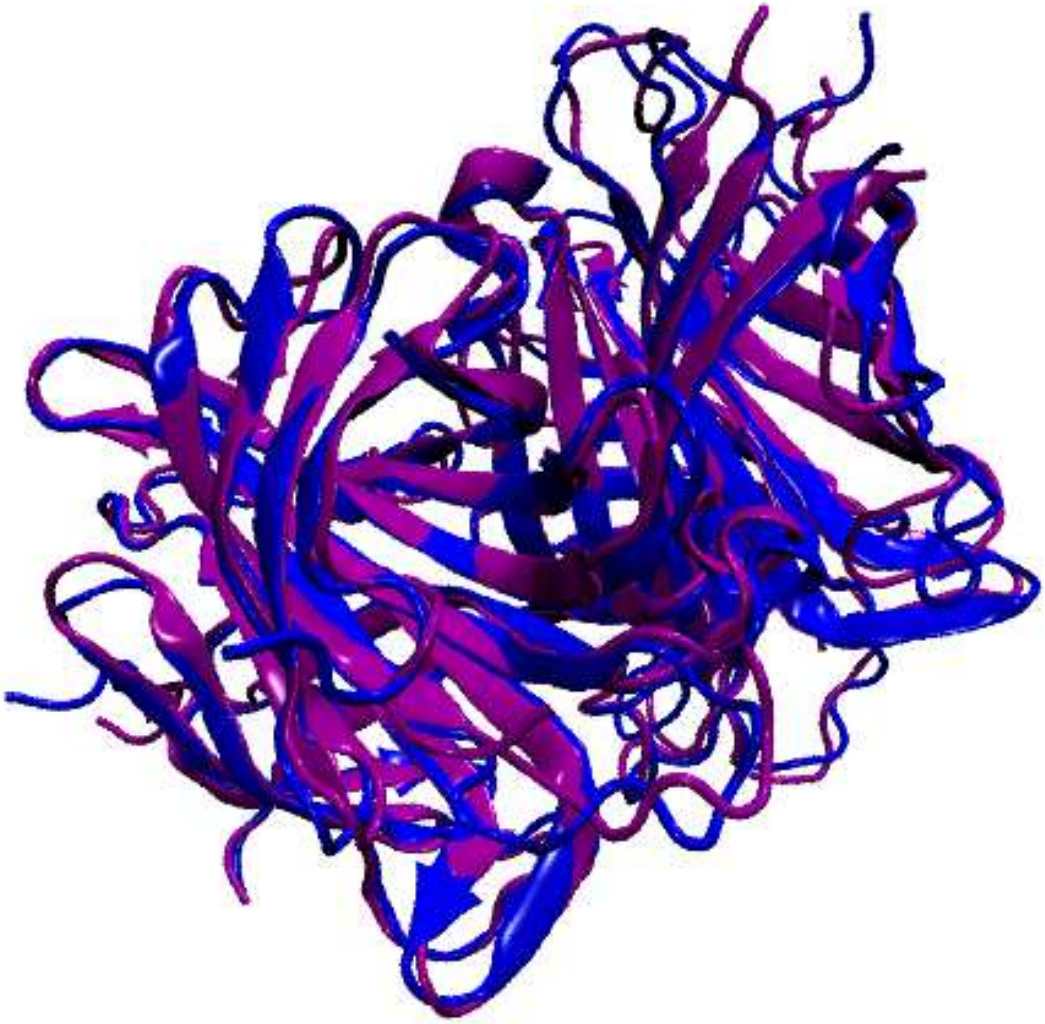

Fig. SI2 Superimposition of WT SAV (blue color) and its mutant S112A (purple color) after the MD run

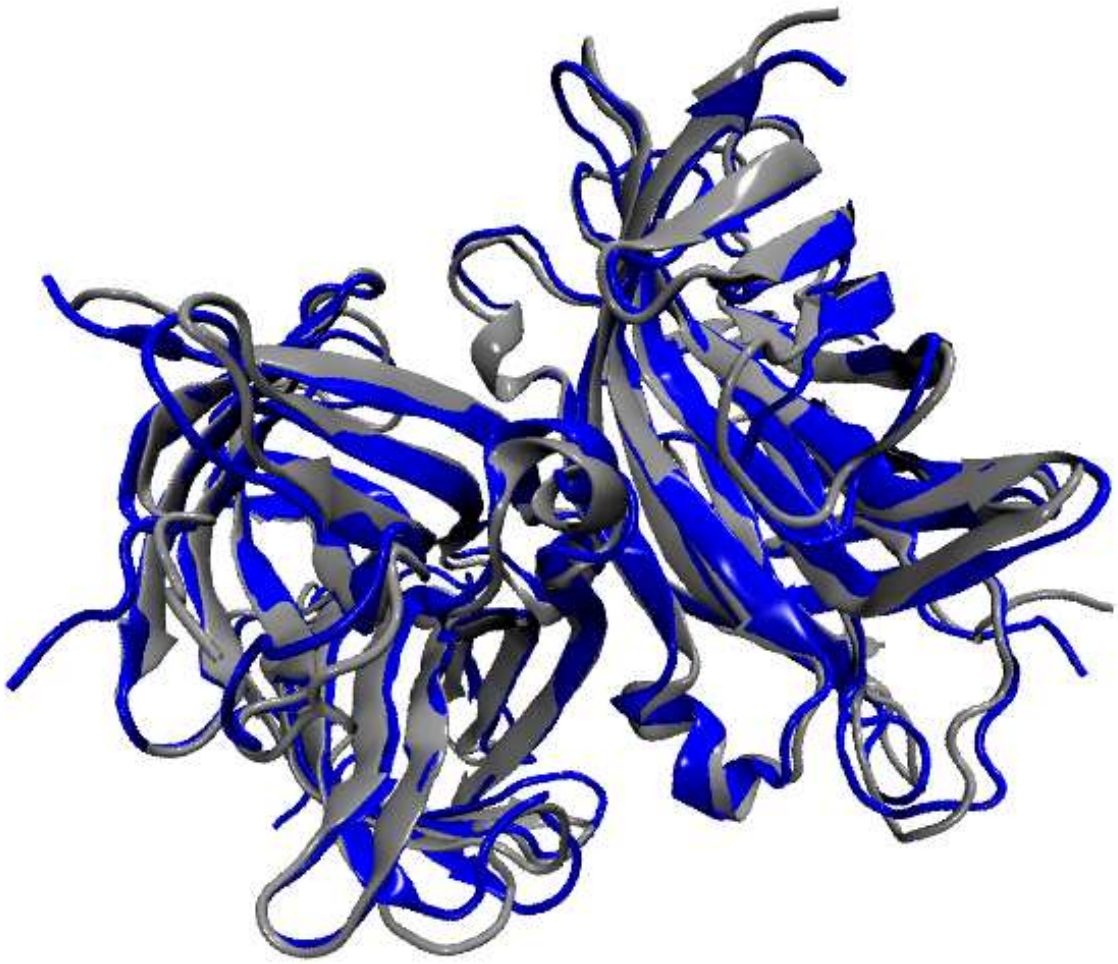

Fig. SI3 Superimposition of WT SAV (blue color) and its S112K (silver color) mutant after the MD run

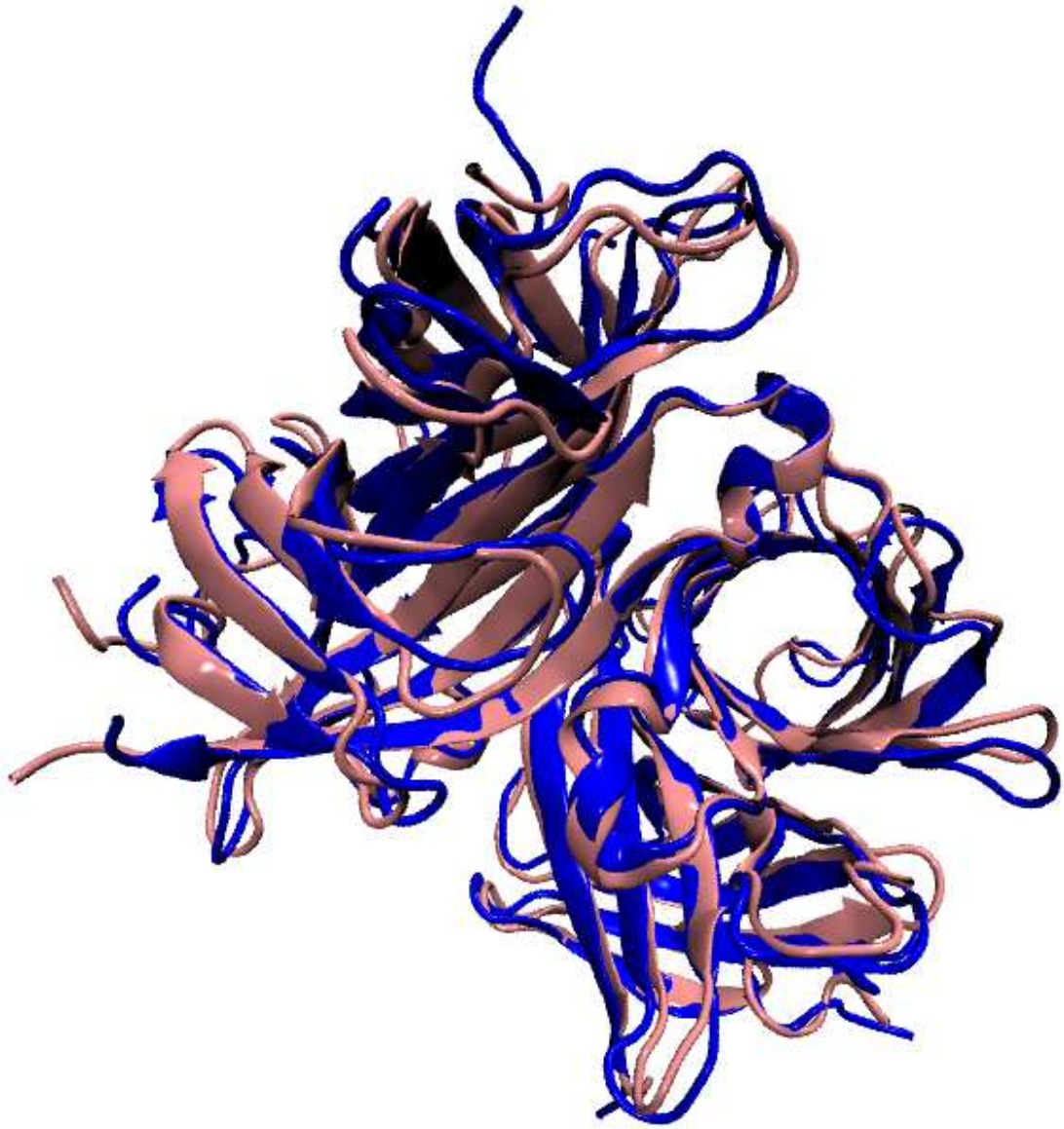

Fig. SI4 Superimposition of WT SAV (blue color) and its P64G (pink color) mutant after the MD run

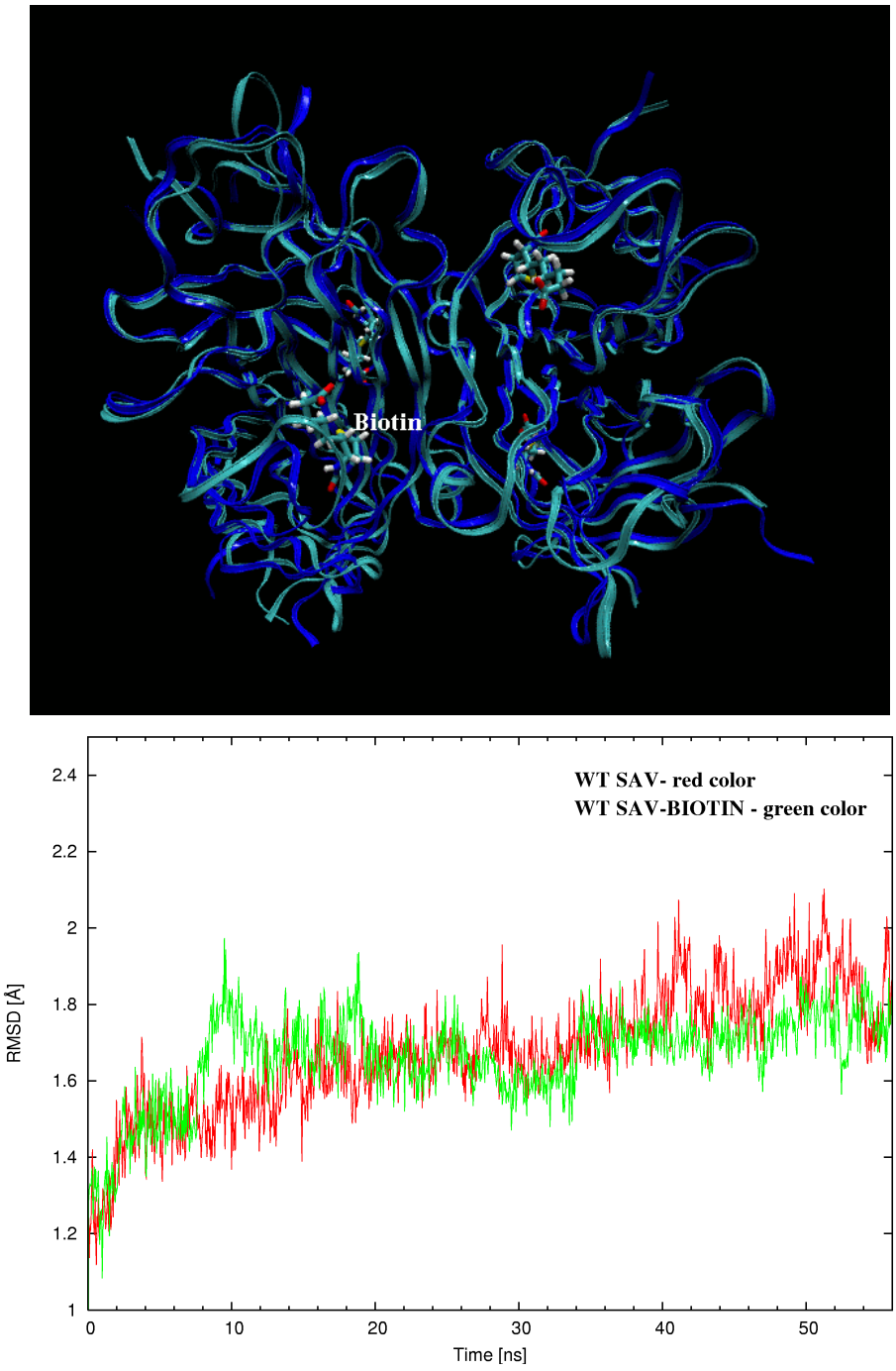

Fig. SI5 Superimposition of WT SAV and WT SAV-Biotin complex (above). WT SAV is marked in blue while WT SAV-Biotin is marked in cyan. In addition the Biotin positions are indicated using licorice. Root mean square deviation (RMSD, in Å) of the protein backbone as a function of MD simulation time (in ns) for WT SAV and WT SAV-Biotin complex is presented (below)

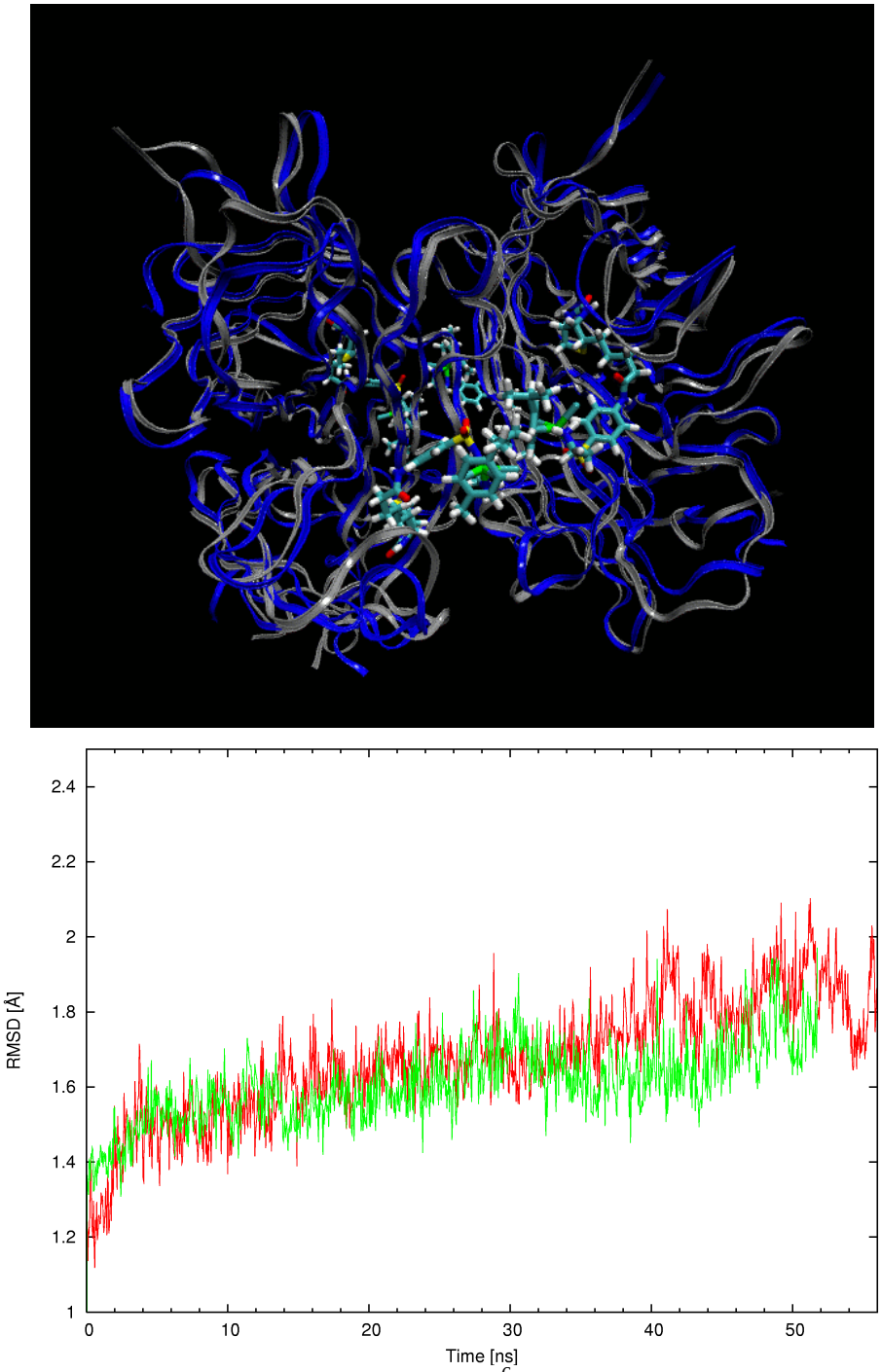

Fig. SI6 Superimposition of WT SAV and WT SAV-[η^6-(p-cymene)Ru(Biot-*p*-L)Cl] complex (above). WT SAV is marked in blue while WT SAV-[η^6-(p-cymene)Ru(Biot-*p*-L)Cl] is marked in silver. In addition, the [η^6-(p-cymene)Ru(Biot-*p*-L)Cl] positions are indicated using licorice. Root mean square deviation (RMSD, in Å) of the protein backbone as a function of MD simulation time (in ns) for WT SAV and WT SAV-[η^6-(p-cymene)Ru(Biot-*p*-L)Cl] complex is presented (below). WT SAV is marked in red while WT SAV-[η^6-(p-cymene)Ru(Biot-*p*-L)Cl] complex is marked in green

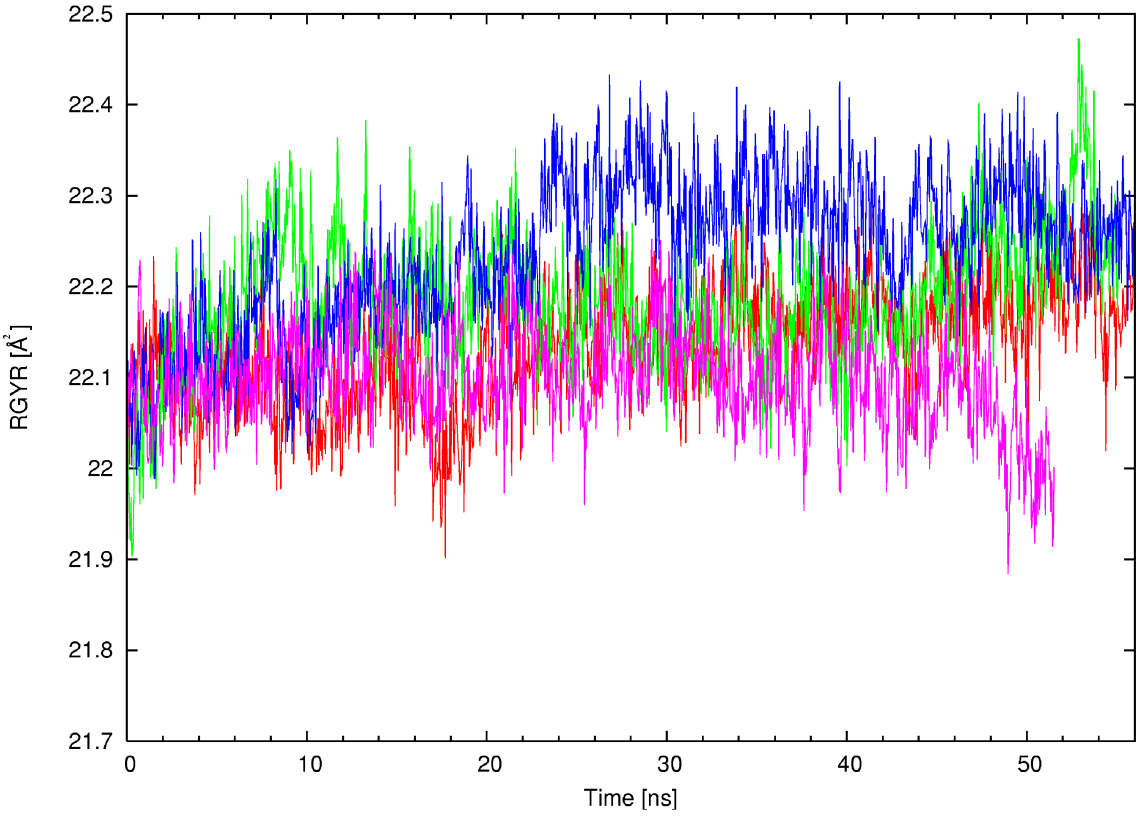

Fig. SI7 Mass-weighted radius of gyration (RGYR) calculated as a function of simulations time for WT SAV and its mutants. WT SAV is marked in red, S112A in green, S112K in blue and P64G in purple

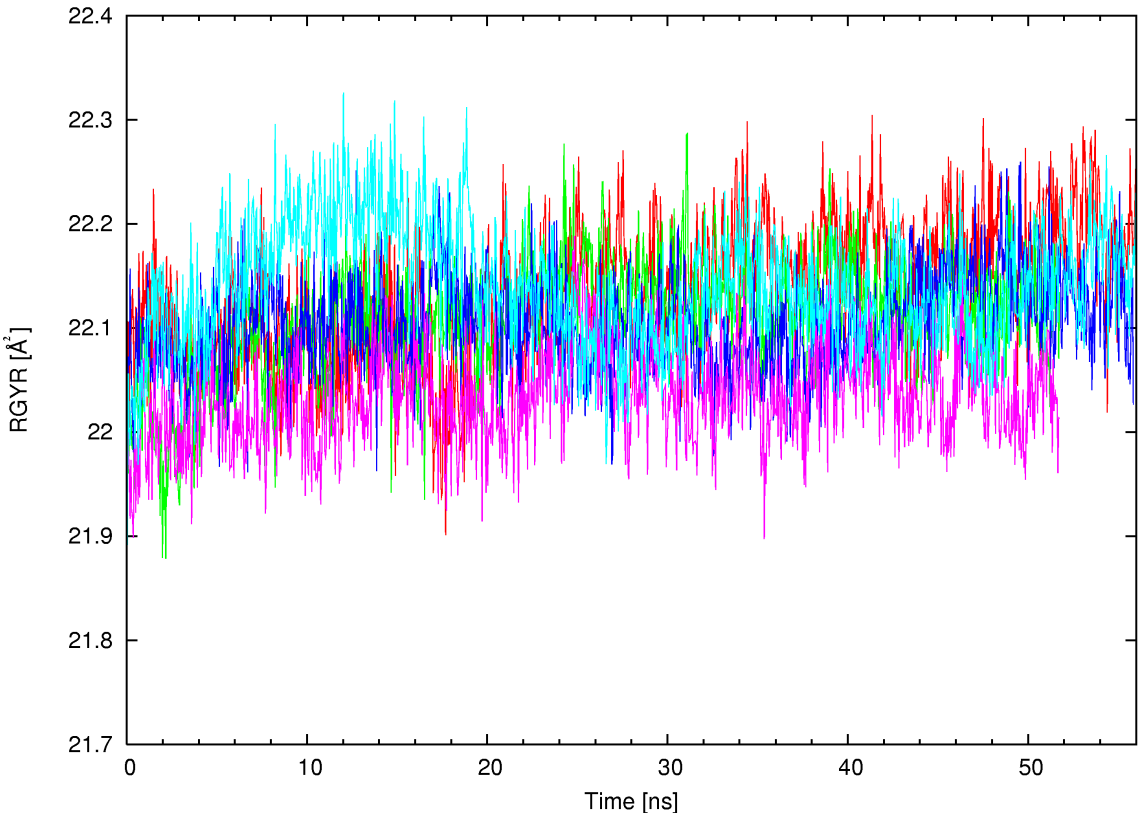

Fig. SI8 Mass-weighted radius of gyration (RGYR) calculated as a function of simulations time for WT SAV, WT SAV-Biotin and its mutants with Biotin. WT SAV is marked in red, WT SAV-Biotin in cyan, S112A-Biotin in green, S112K-Biotin in blue and P64G-Biotin in purple

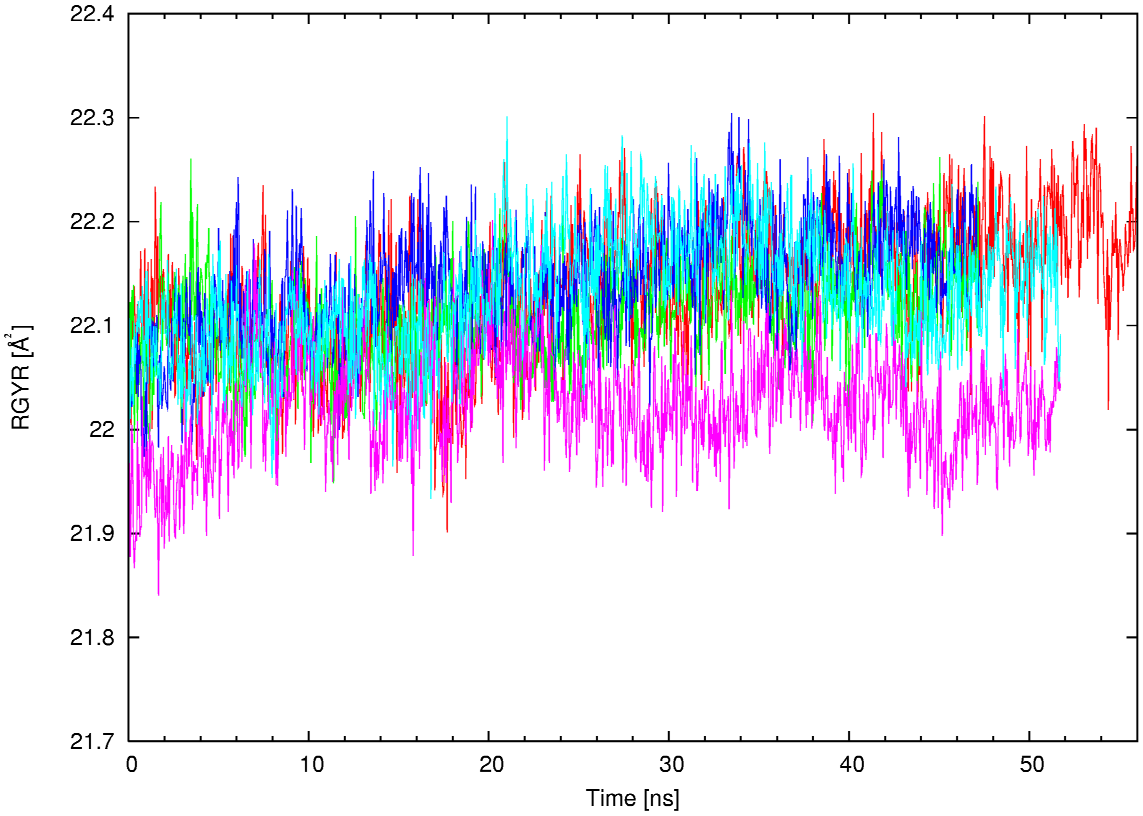

Fig. SI9 Mass-weighted radius of gyration (RGYR) calculated as a function of simulations time for WT SAV, WT SAV-[η^6-(*p*-cymene)Ru(Biot-*p*-L)Cl] and its mutants with [η^6-(*p*-cymene)Ru(Biot-*p*-L)Cl]. WT SAV is marked in red, WT SAV-[η^6-(*p*-cymene)Ru(Biot-*p*-L)Cl] in cyan, S112A-[η^6-(*p*-cymene)Ru(Biot-*p*-L)Cl] in green, S112K-[η^6-(*p*-cymene)Ru(Biot-*p*-L)Cl] in blue and P64G-[η^6-(*p*-cymene)Ru(Biot-*p*-L)Cl] in purple

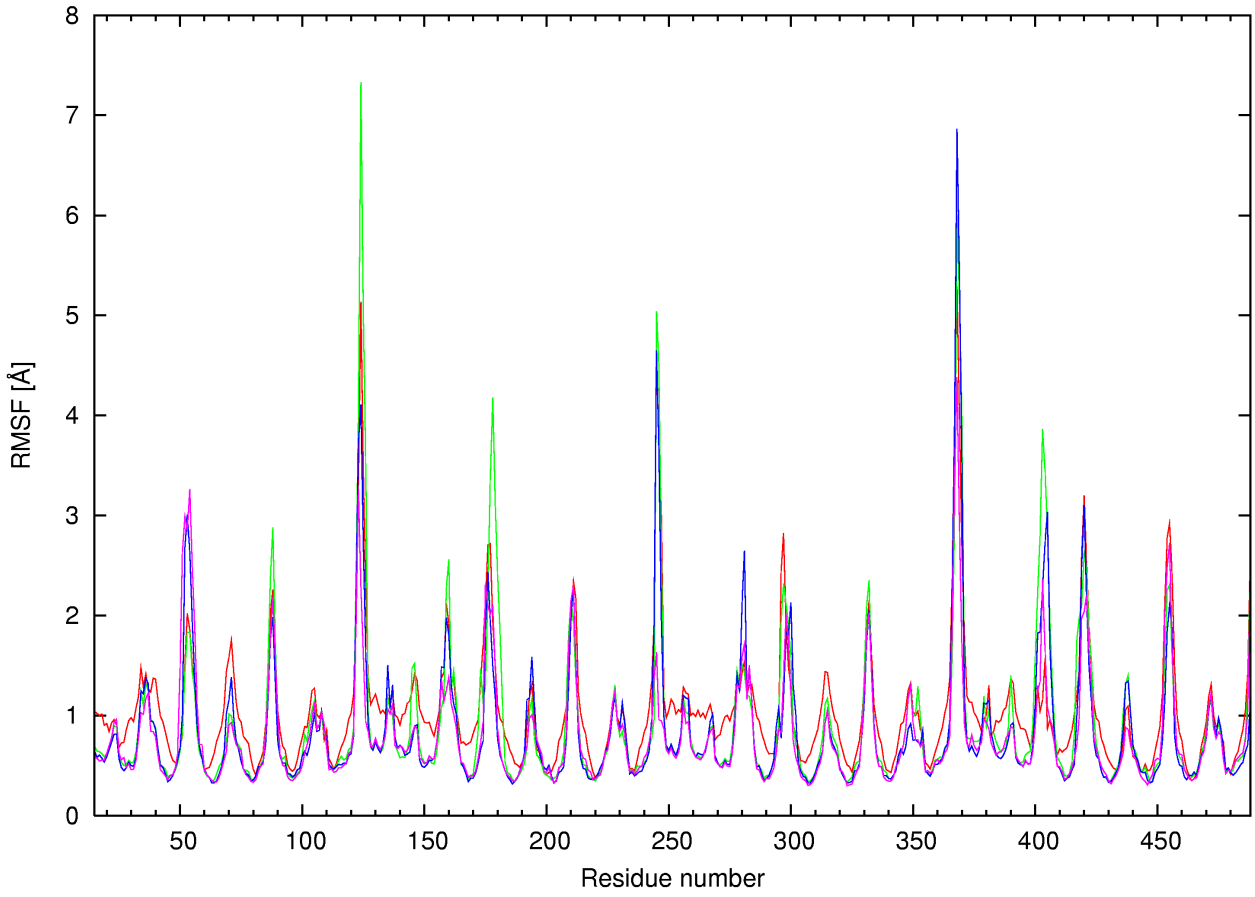

Fig. SI10 Root Mean Square Fluctuation (RMSF) of the backbone atoms of individual residues of WT SAV and its mutants. WT SAV is marked in red, S112A in green, S112K in blue and P64G in purple

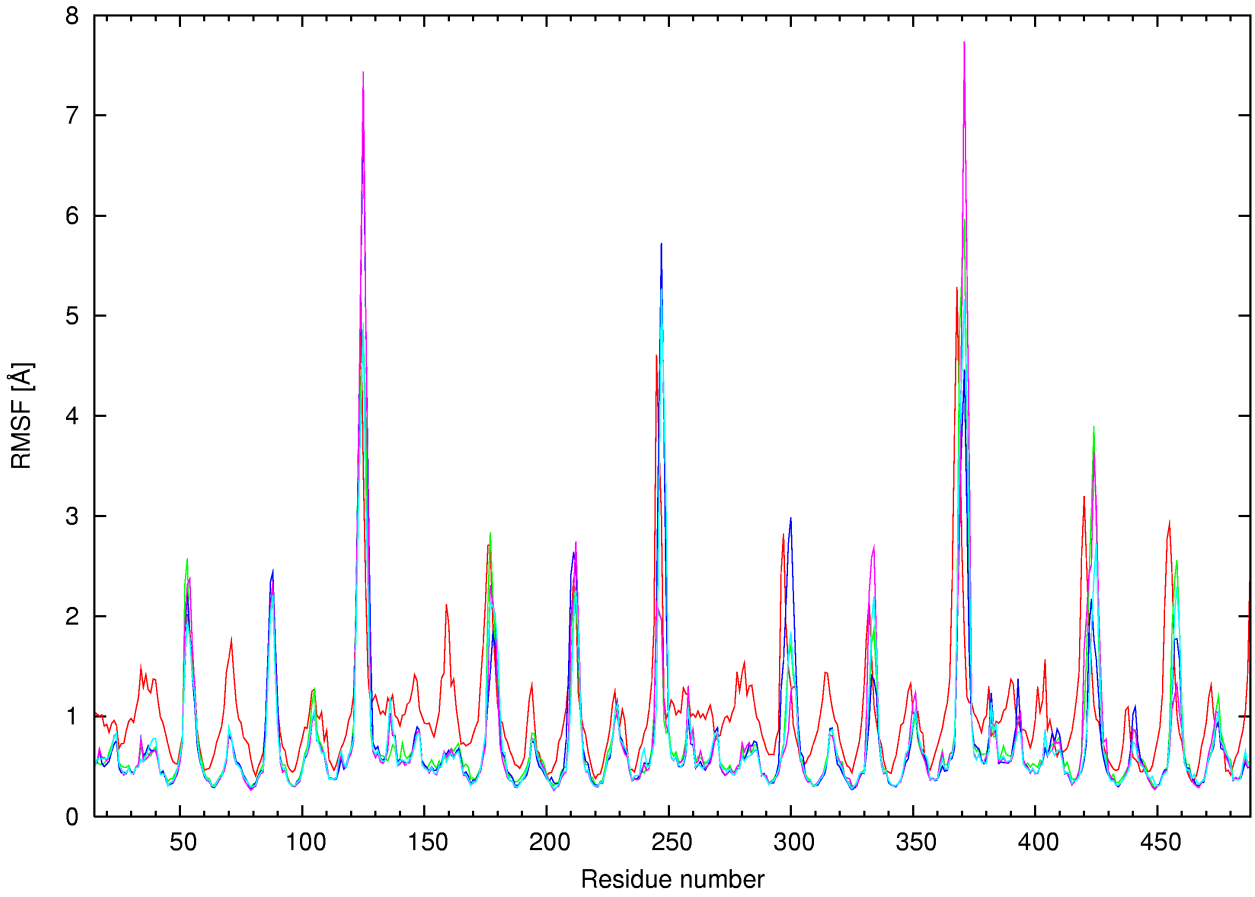

Fig. SI11 Root Mean Square Fluctuation (RMSF) of the backbone atoms of individual residues of WT SAV, WT SAV-Biotin complex and mutants with Biotin. WT SAV is marked in red, WT SAV-Biotin in cyan, S112A-Biotin in green, S112K-Biotin in blue and P64G-Biotin in purple

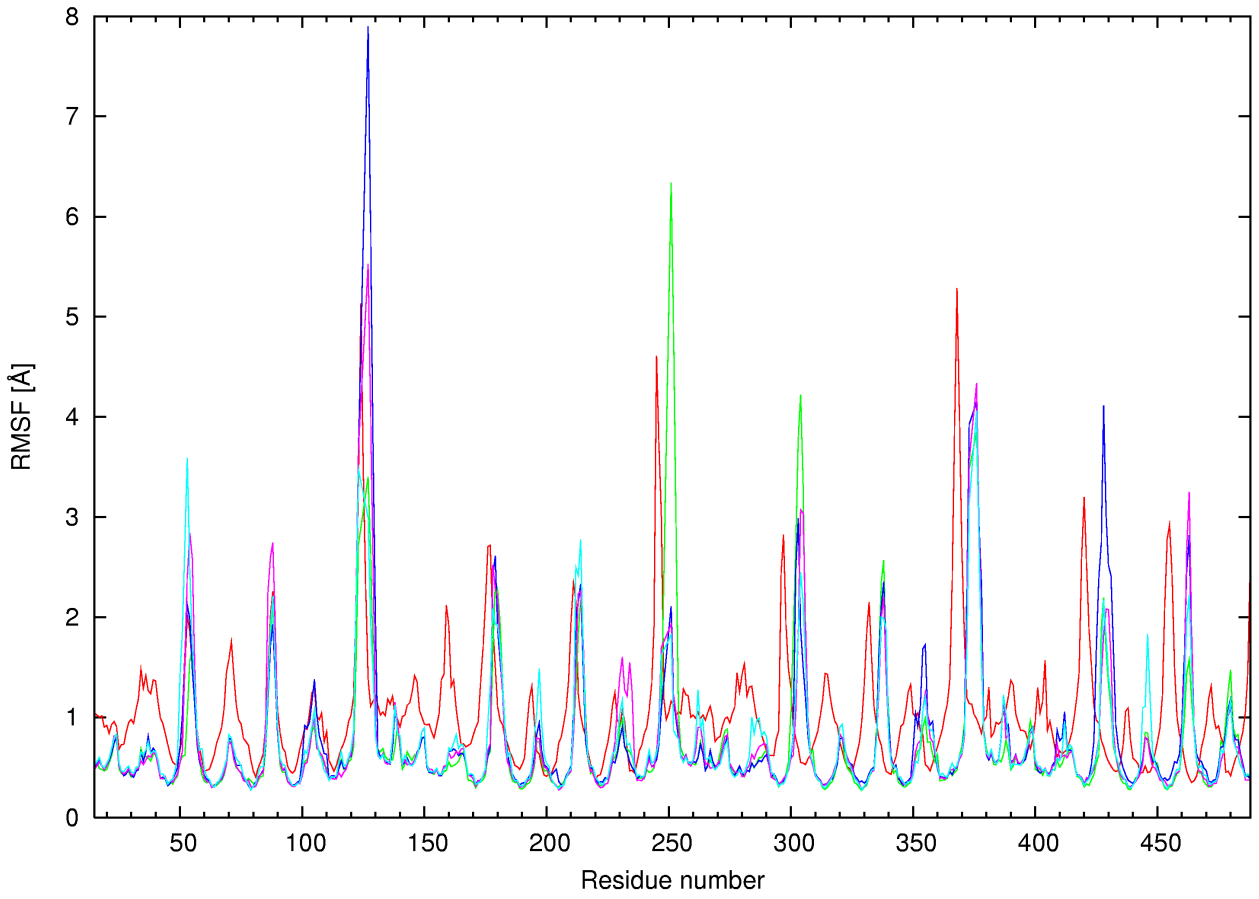

Fig. SI12 Root Mean Square Fluctuation (RMSF) of the backbone atoms of individual residues of WT SAV, WT SAV-[η^6-(p-cymene)Ru(Biot-*p*-L)Cl] complex and mutants with [η^6-(p-cymene)Ru(Biot-*p*-L)Cl]. WT SAV is marked in red, WT SAV-[η^6-(p-cymene)Ru(Biot-*p*-L)Cl] in cyan, S112A-[η^6-(p-cymene)Ru(Biot-*p*-L)Cl] in green, S112K-[η^6-(p-cymene)Ru(Biot-*p*-L)Cl] in blue and P64G-[η^6-(p-cymene)Ru(Biot-*p*-L)Cl] in purple

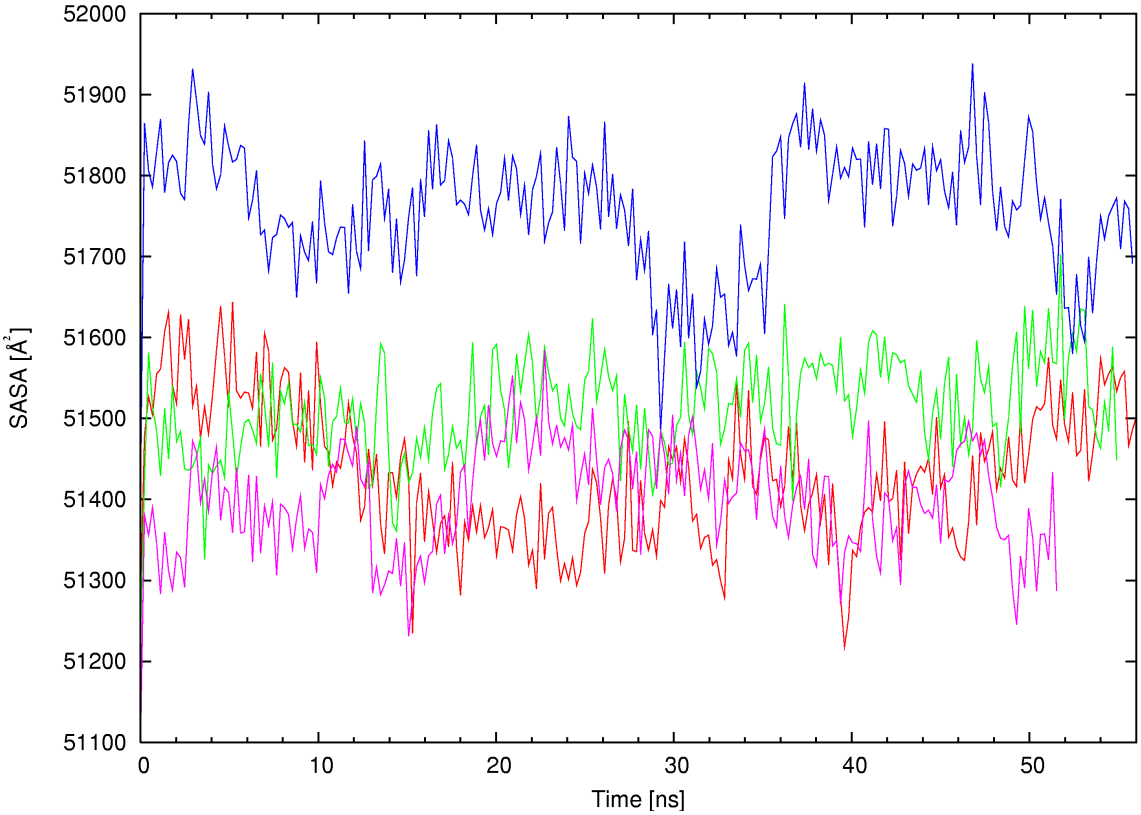

Fig. SI13 Solvent accessible surface area (SASA) calculated as a function of simulation time for WT SAV and its mutants. WT SAV is marked in red, S112A in green, S112K in blue and P64G in purple

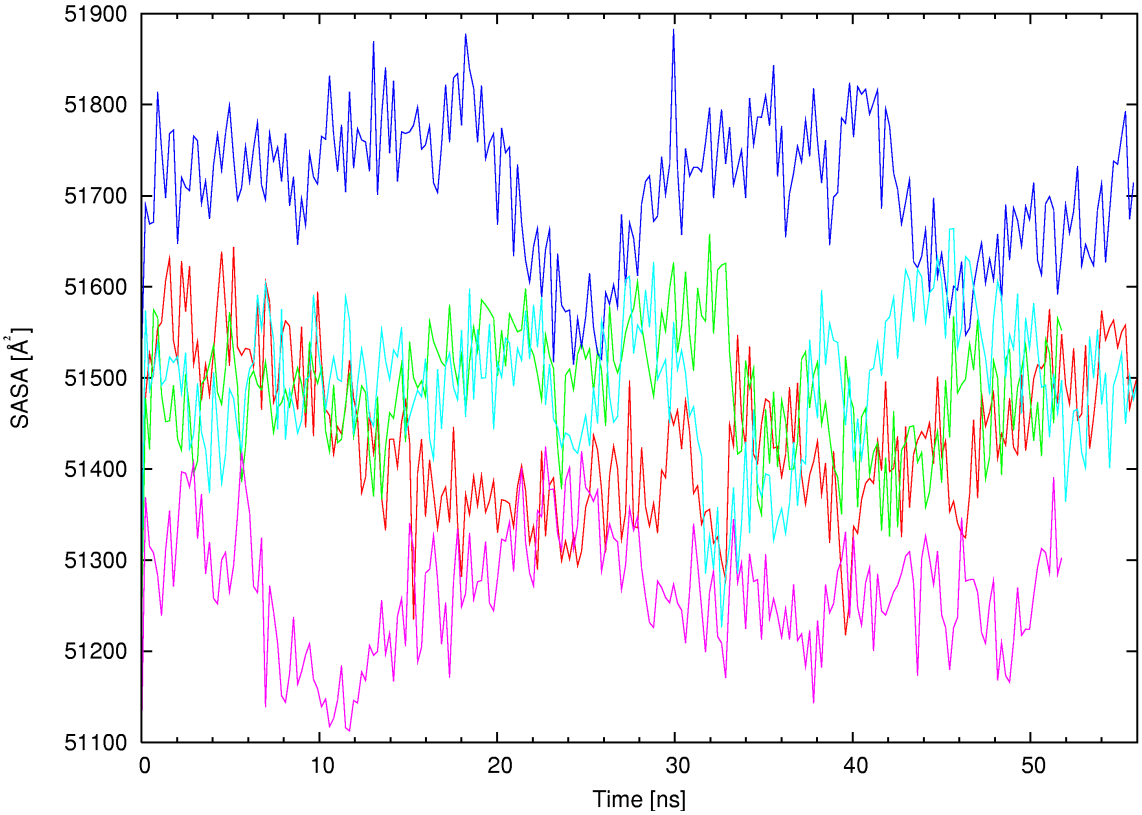

Fig. SI14 Solvent accessible surface area (SASA) calculated as a function of simulation time for WT SAV and WT SAV-Biotin and its mutants with Biotin. WT SAV is marked in red, WT SAV-Biotin in cyan, S112A-Biotin in green, S112K-Biotin in blue and P64G-Biotin in purple

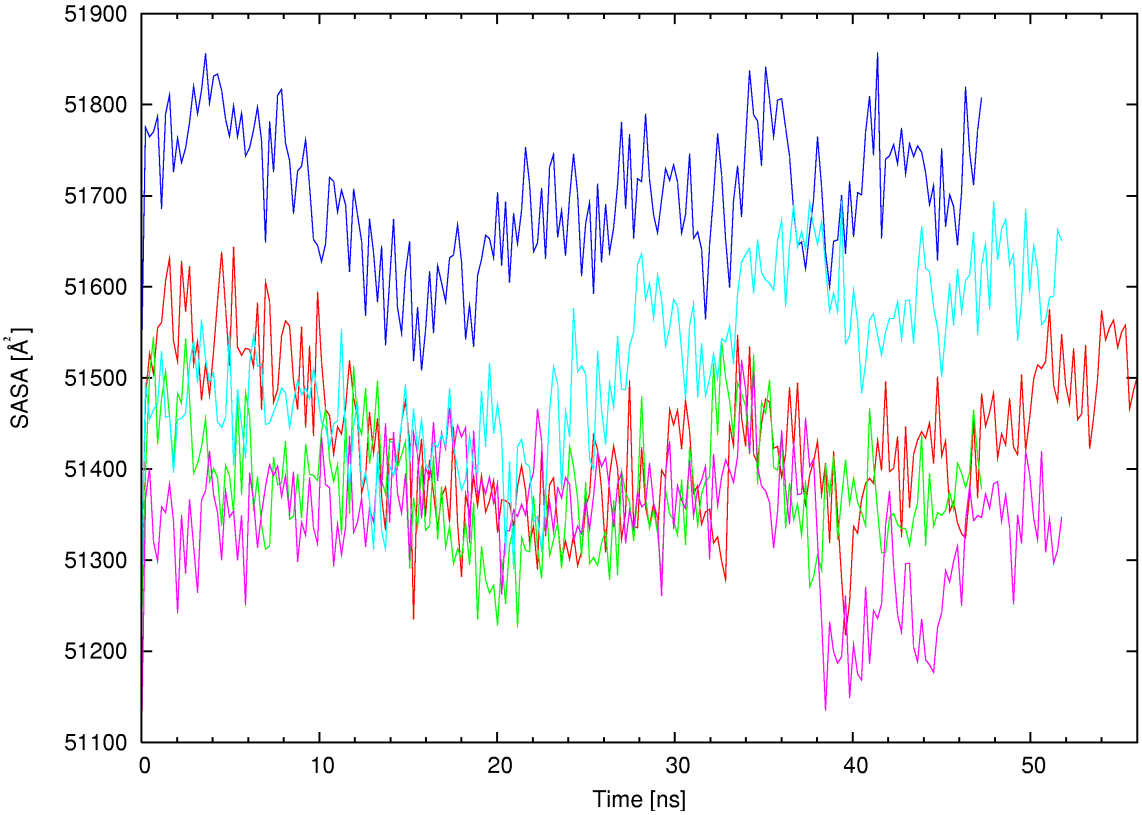

Fig. SI15 Solvent-accessible surface area (SASA) calculated as a function of simulation time for WT SAV, WT SAV-[η^6-(*p*-cymene)Ru(Biot-*p*-L)Cl] and its mutants with [η^6-(*p*-cymene)Ru(Biot-*p*-L)Cl]. WT SAV is marked in red, WT SAV-[η^6-(*p*-cymene)Ru(Biot-*p*-L)Cl] in cyan, S112A-[η^6-(*p*-cymene)Ru(Biot-*p*-L)Cl] in green, S112K-[η^6-(*p*-cymene)Ru(Biot-*p*-L)Cl] in blue and P64G-[η^6-(*p*-cymene)Ru(Biot-*p*-L)Cl] in purple

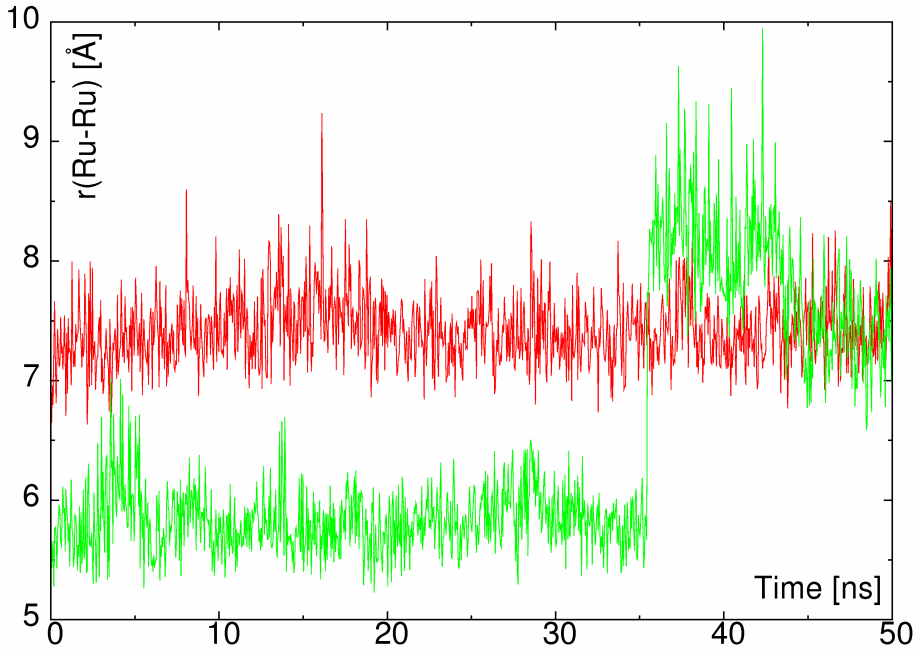

Fig. SI16 Time evolution of the Ru-Ru distances for metals in neighboring η^6-(p-cymene)Ru(Biot-*p*-L)Cl ligands anchored in WT SAV. Results of classical MD. Stereochemistry of the metal centers: the *R* – *R* pair is marked green, the *R* – *S* pair is marked red. Average distances and their standard deviations: 6.45±0.99Å for the *R* – *R*, 7.48±0.30Å for the *R* – *S*

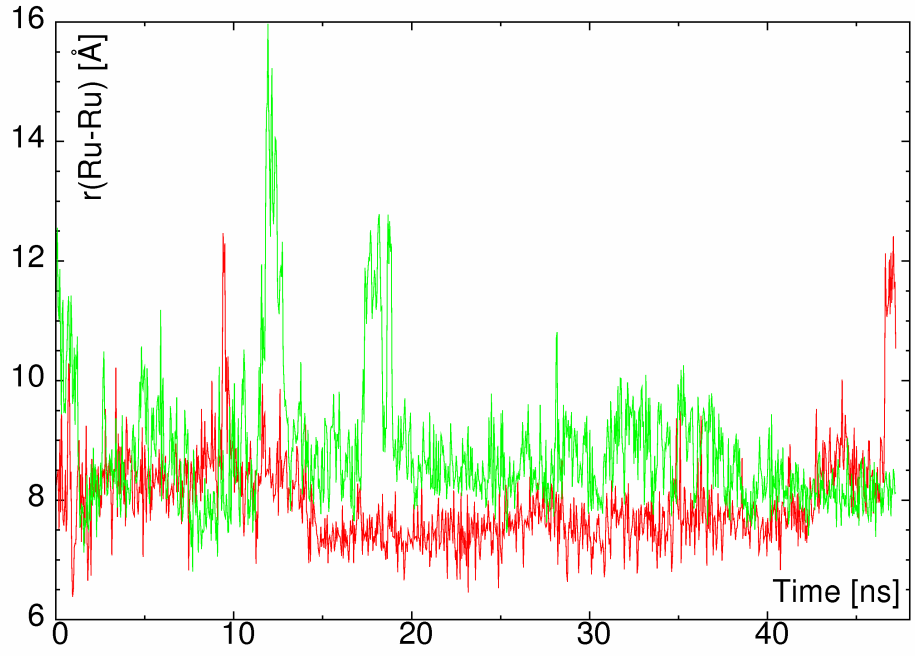

Fig. SI17 Time evolution of the Ru-Ru distances for metals in neighboring η^6-(p-cymene)Ru(Biot-*p*-L)Cl ligands anchored in S112A-SAV. Results of classical MD. Stereochemistry of the metal centers: the *R* – *R* pair is marked green, the *R* – *S* pair is marked red. Average distances and their standard deviations: 8.81±1.13Å for the *R* – *R*, 7.96±0.78Å for the *R* – *S*

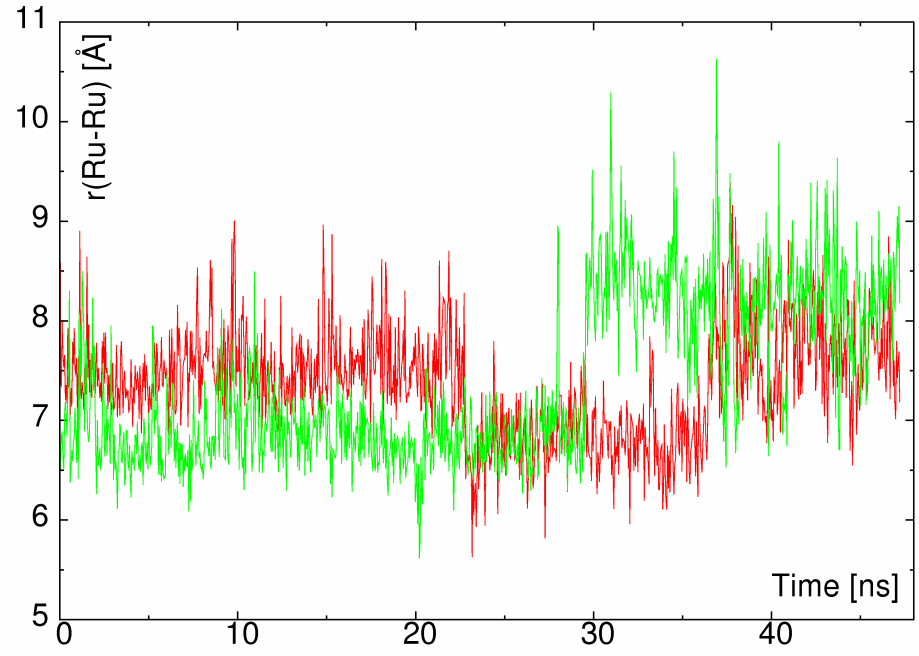

Fig. SI18 Time evolution of the Ru-Ru distances for metals in neighboring η^6-(p-cymene)Ru(Biot-*p*-L)Cl ligands anchored in S112K-SAV. Results of classical MD. Stereochemistry of the metal centers: the *R* – *R* pair is marked green, the *R* – *S* pair is marked red. Average distances and their standard deviations: 7.38±0.81Å for the *R* – *R*, 7.36±0.55Å for the *R* – *S*

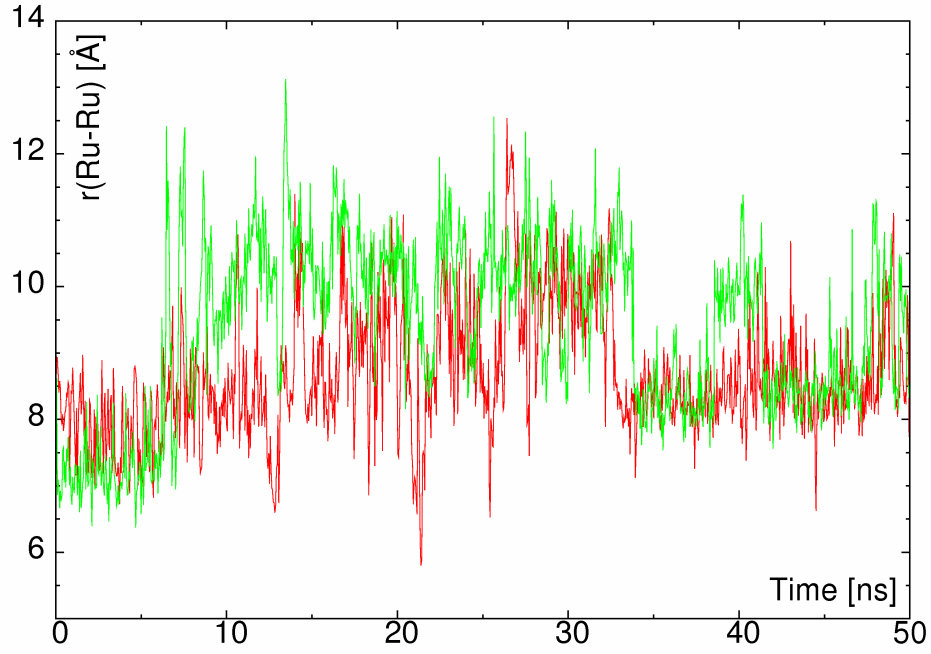

Fig. SI19 Time evolution of the Ru-Ru distances for metals in neighboring η^6-(p-cymene)Ru(Biot-*p*-L)Cl ligands anchored in P64G-SAV. Results of classical MD. Stereochemistry of the metal centers: the *R* – *R* pair is marked green, the *R* – *S* pair is marked red. Average distances and their standard deviations: 9.34±1.29Å for the *R* – *R*, 8.67±0.97Å for the *R* – *S*

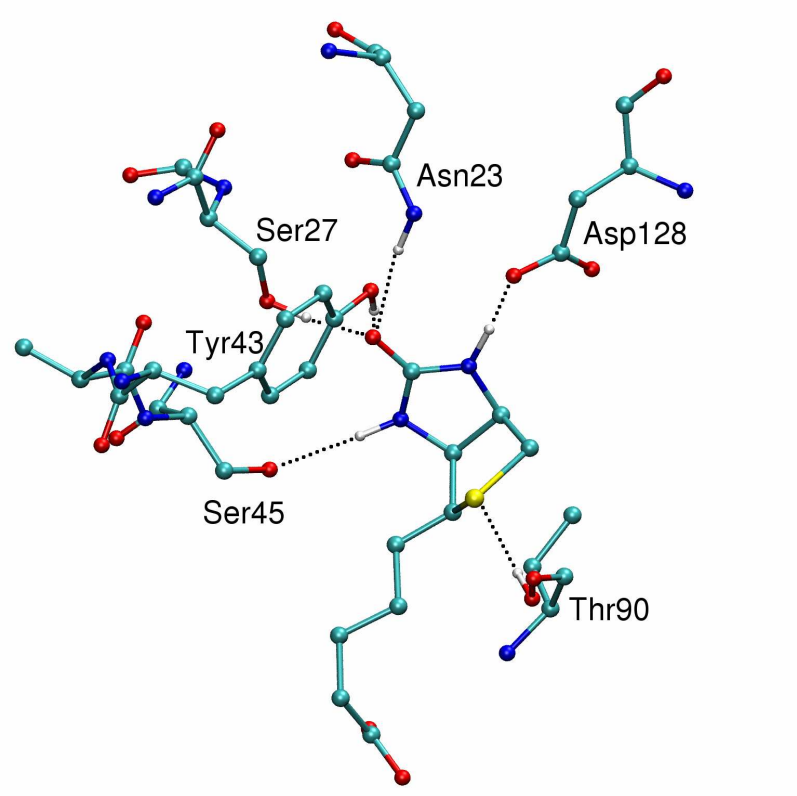

Fig. SI20 Additional view of the biotin surrounded by selected residues forming hydrogen bonding network – a model for *ab initio* Born-Oppenheimer Molecular Dynamics. For clarity, only those hydrogen atoms which participate in the hydrogen bonds are visualized

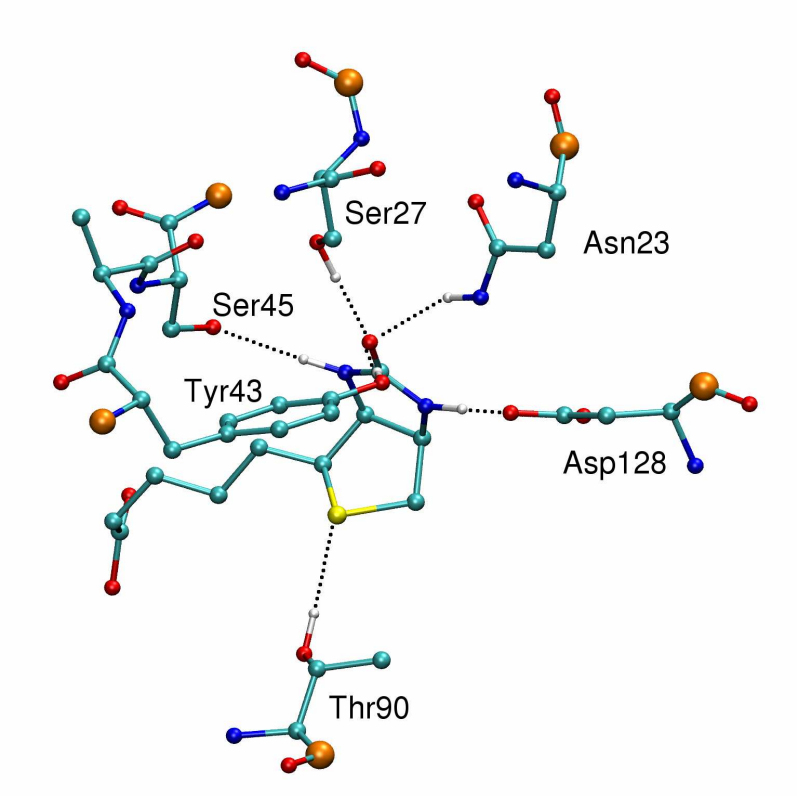

Fig. SI21 Additional view of the biotin surrounded by selected residues forming hydrogen bonding network – a model for *ab initio* Born-Oppenheimer Molecular Dynamics. Fixed atoms (on which the position constraints were assumed during initial optimization and MD run) are marked with orange spheres

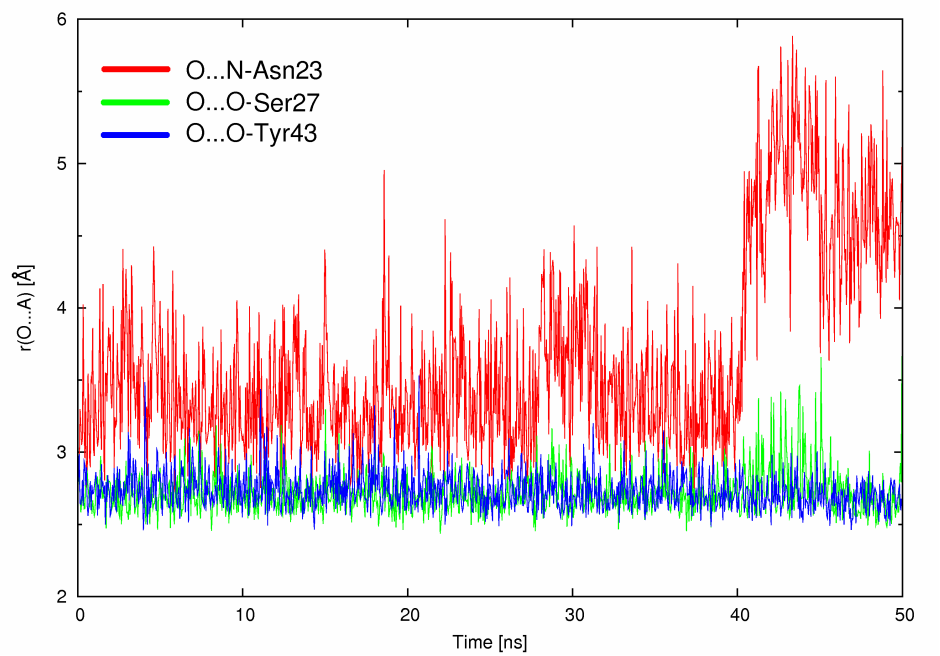

Fig. SI22 Time evolution of the hydrogen bonds with carbonyl oxygen atom of biotin acting as an acceptor. Results of classical force field molecular dynamics for the P64G SAV mutant loaded with the metal-bearing cofactor. The behavior is typical for other models as well: the contact to Asn23 is less stable than the remaining two hydrogen bonds.

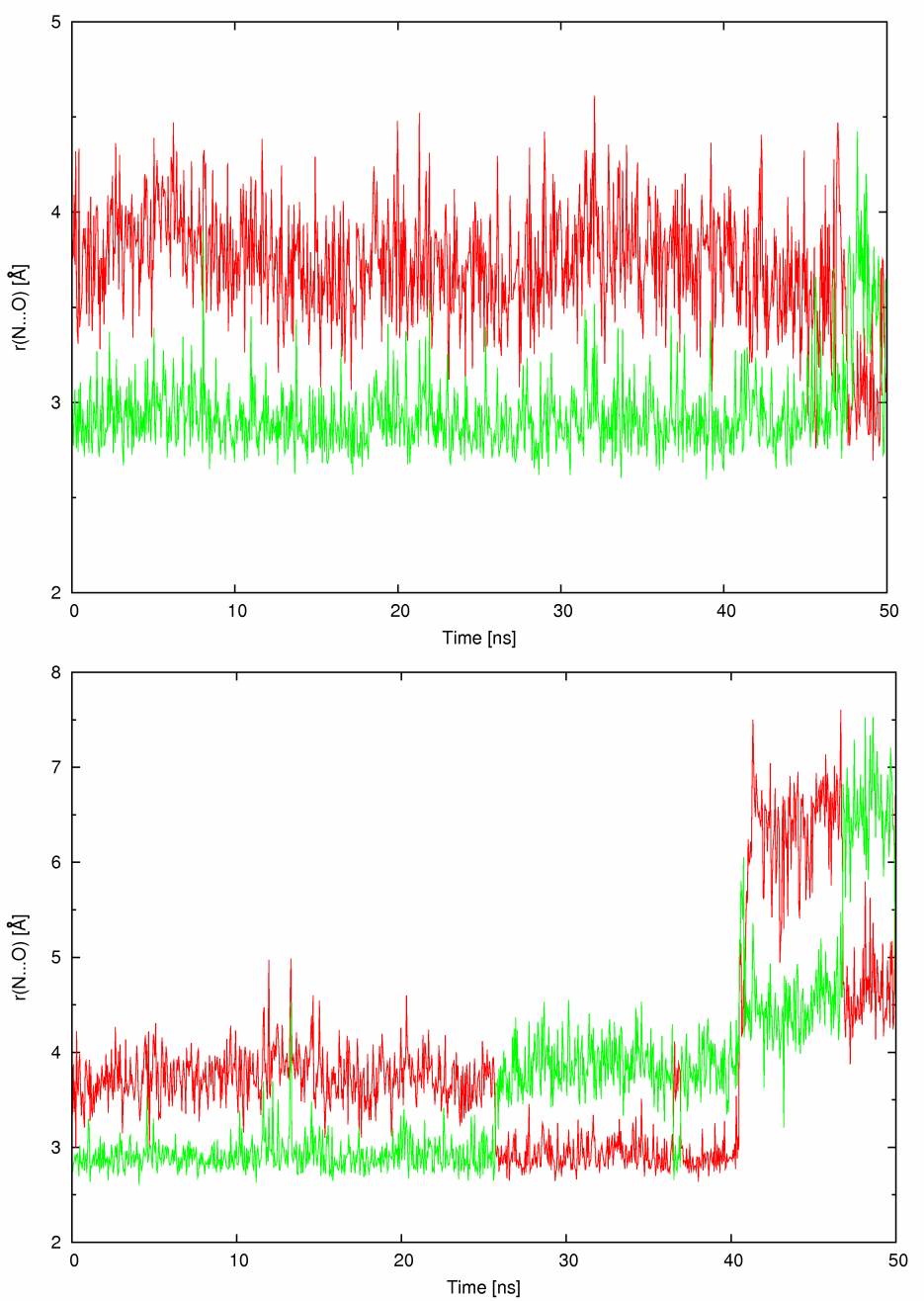

Fig. SI23 Time evolution of the hydrogen bonds with the N2 ureido nitrogen atom of biotin acting as a donor. The acceptor atoms are two carboxyl oxygens of Asp128 (distinguishable by red and green graphs). Results of classical force field molecular dynamics for the S112K SAV mutant loaded with the metal-bearing cofactor. Typically also for other simulations, this bond can be unstable for one binding pocket (lower panel), while it is conserved for the other ones (upper panel). Note that both oxygen atoms of the Asp128-COO^- can serve as acceptors and exchange their role during the simulation.

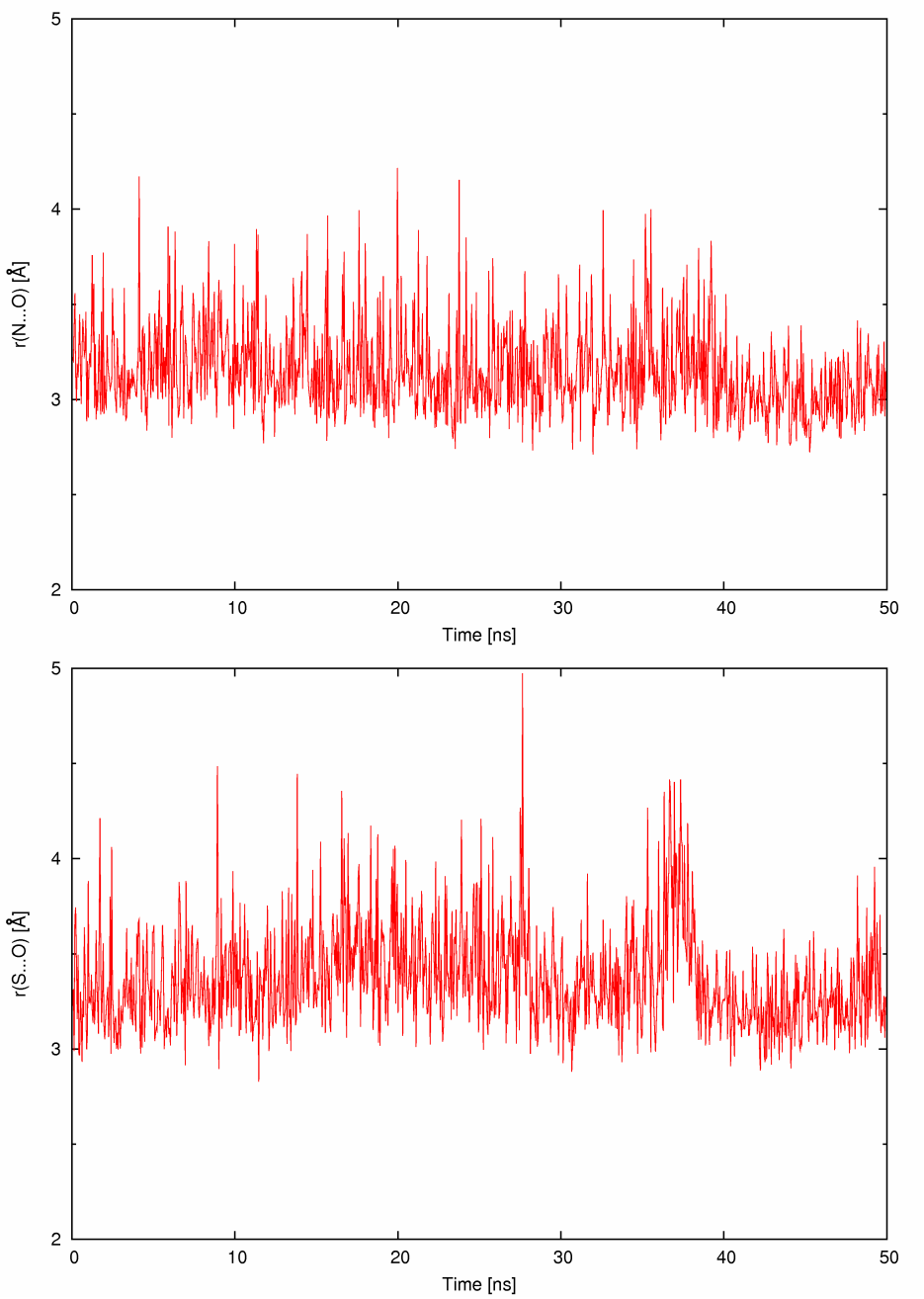

Fig. SI24 Time evolution of the two hydrogen bonds: with the N1 ureido nitrogen atom of biotin acting as a donor (N1-H…O-Ser45, upper panel) and the sulfur atom of the biotin acting as an acceptor (Ser90-O-H…S, lower panel). Results of classical force field molecular dynamics for the S112K SAV mutant loaded with the metal-bearing cofactor. These bonds are stable in the simulations.